Atmospheric
Chemistry
and Physics
Discussions

1 **Differences between recent emission inventories strongly affect anthropogenic aerosol**
2 **evolution from 1990 to 2019**

3 Marianne T. Lund[1,*], Gunnar Myhre[1], Ragnhild B. Skeie[1], Bjørn H. Samset[1], Zbigniew Klimont[2]

4

5 1 CICERO Center for International Climate Research, Oslo, Norway

6 2 International Institute for Applied Systems Analysis (IIASA), Laxenburg, Austria

7 *Corresponding author: m.t.lund@cicero.oslo.no

8

9 **Abstract**

10 *This study focuses on implications of differences between recent global emissions inventories for*
11 *simulated trends in anthropogenic aerosol abundances and radiative forcing (RF) over the 1990-2019*
12 *period. We use the ECLIPSE version 6 (ECLv6) and Community Emission Data System year 2021*
13 *release (CEDS21) as input to the chemical transport model OsloCTM3 and compare the resulting*
14 *aerosol evolution to corresponding results derived with the first CEDS release, as well as to observed*
15 *trends in regional and global aerosol optical depth (AOD). Using CEDS21 and ECLv6 results in 3%*
16 *and 6% lower global mean AOD compared to CEDS in 2014, primarily driven by differences over China*
17 *and India, where the area average AOD is up to 30% lower. These differences are considerably larger*
18 *than the satellite-derived interannual variability in AOD. A negative linear trend (over 2005-2017) in*
19 *global AOD following changes in anthropogenic emissions is found with all three inventories but is*
20 *markedly stronger with CEDS21 and ECLv6. Furthermore, we confirm that the model better captures*
21 *the sign and strength of the observed AOD trend over China with CEDS21 and ECLv6 compared to*
22 *using CEDS. We estimate a net, global mean aerosol-induced RF in 2014 relative to 1990 of 0.08 W m^{-2}*
23 *for CEDS21, and 0.12 W m^{-2} for ECLv6, compared to 0.03 W m^{-2} with CEDS. Using CEDS21, we also*
24 *estimate the RF in 2019 relative to 1990 to be 0.10 W m^{-2}, reflecting the continuing decreasing trend in*
25 *aerosol loads post 2014. Our results facilitate more rigorous comparison between existing and*
26 *upcoming studies of climate and health effects of aerosols using different emission inventories.*

27

28 **1 Introduction**

29 Human activities have led to a substantial increase in atmospheric abundances of aerosols relative to
30 pre-industrial conditions. While increasing emissions of greenhouse gases is the dominant driver of
31 recent global warming, aerosols play a key role in shaping regional and global climate, and for
32 anthropogenic climate change, through their interactions with radiation and clouds. The sixth assessment
33 report (AR6) of the Intergovernmental Panel on Climate Change (IPCC) estimates that changes in
34 atmospheric aerosols have contributed an effective radiative forcing (ERF) of −1.3 W m^{-2} over the
35 industrial era (1750–2014), albeit with a wide uncertainty range of −2.0 to −0.6 W m^{-2} (Forster et al.,
36 2021).

37 Over recent decades, anthropogenic emissions of aerosols and their precursor gases has been changing
38 rapidly, with substantial spatiotemporal heterogeneity and particularly in Asia. Following decades of
39 rapid economic growth in China, the combustion of coal, other fossil fuels, and biofuels increased
40 considerably, resulting in the region becoming the dominating source of air pollution emissions.
41 However, since the implementation of the Action Plan on Air Pollution Prevention and Control,
42 emissions of sulfur dioxide (SO_2) and then nitrogen oxide (NOx) in China have declined rapidly

43   (Klimont et al., 2017; Klimont et al., 2013; Tong et al., 2020; Zheng et al., 2018). Recent studies suggest
44   that also black carbon (BC) emissions are declining (Kanaya et al., 2020; Zheng et al., 2018). In contrast,
45   a continuing strong growth of SO_2 emissions has been seen in South Asia (Kurokawa & Ohara, 2020;
46   Li et al., 2017). These contrasting trends have given rise to a distinct dipole pattern of increasing and
47   declining aerosol optical depth over South and East Asia, respectively, visible in satellite data (Samset
48   et al., 2019).

49   Such rapid aerosol changes are likely to affect regional climate, however the exact magnitude and role
50   remains insufficiently quantified. One factor contributing to uncertainty is the substantial differences,
51   in both magnitudes and trends, that exist between current emission inventories (e.g. Crippa et al., 2018;
52   Elguindi et al., 2020). A critical issue that has recently been highlighted is a notable underestimation of
53   the decline in Chinese emissions of SO_2 and NOx, and overestimation of carbonaceous aerosol
54   emissions in Asia and Africa, in the Community Emission Data System (CEDS) developed for the sixth
55   cycle of the Coupled Model Intercomparison Project (CMIP6) (Szopa et al., 2021). Since the initial parts
56   of the CMIP6 exercise, the CEDS inventory has undergone several revisions. The most recent version,
57   CEDS21, covering the period up to 2019, exhibit several key differences compared to the initial release
58   – for some species all the way back to the early 2000s (O'Rourke et al. (2021)). In particular, both BC
59   and OC emissions are substantially lower in the update, and issues related to the decreasing trend in
60   Chinese SO_2 are largely addressed.

61   Given the relative importance of these source regions, such inventory differences may have implications
62   for simulations of anthropogenic aerosol distributions globally and contribute to increased uncertainty
63   in estimates of aerosol-induced climate impacts, both in the IPCC AR6 and elsewhere in the literature.
64   For instance, recent work has shown that results from the CMIP6 experiments fail to fully capture the
65   observed recent trends in aerosol optical depth (AOD) in Asia (Cherian & Quaas, 2020; Ramachandran
66   et al., 2022; Su et al., 2021; Wang et al., 2021), with the discrepancy largely attributed to the
67   misrepresentation of emissions in the region in last decade of the historical CMIP6 period. Other studies
68   demonstrate that the poor representation of observed aerosol trends can propagate to further
69   uncertainties in attribution of aerosol-induced impacts, such as the East Asian monsoon (Wang et al.,
70   2022) and health impacts (Cheng et al., 2021). In addition to CMIP6, the CEDS emissions have also
71   been used in individual model studies of historical aerosol evolution, radiative forcing, sector attribution,
72   and air quality assessments (e.g. Bauer et al., 2020; Chowdhury et al., 2022; Lund et al., 2018; Lund et
73   al., 2020; Paulot et al., 2018). Moreover, uncertainties and biases in the baseline historical inventory
74   may influence scenario-based assessments of near-term future regional climate risk.

75   As the update to CEDS came too late for uptake in IPCC AR6, it is pertinent to investigate the influence
76   of the emission differences on the modeled evolution of atmospheric aerosol trends and subsequent
77   climate implications. Here we undertake one such investigation. Using the chemical transport model
78   OsloCTM3, we perform simulations with the CEDS21 emission inventory and compare to previously
79   published results derived with the original CEDS release (Lund et al., 2018; Lund et al., 2019). We also
80   perform simulations with a third recent global inventory, the ECLIPSE version 6b, where emissions are
81   similar in evolution but generally even lower than in CEDS21, especially in the most recent period. We
82   quantify the differences between inventories in simulated evolution of global and regional
83   anthropogenic aerosol loads over the 1990-2014 period and in the resulting radiative forcing. We also
84   explore the post-2014 aerosol evolutions with CEDS21 and compare trends in simulated aerosol optical
85   depth to remote sensing observations.

86

2 Methods

88   Atmospheric concentrations of aerosols are simulated with the global chemical transport model
89   OsloCTM3 (Lund et al., 2018; Søvde et al., 2012). The model is driven by meteorological data from the

90   European Center for Medium Range Weather Forecast (ECMWF) OpenIFS model updated every 3
91   hours and is run in a 2.25°x2.25° horizontal resolution, with 60 vertical levels (the uppermost centered
92   at 0.1 hPa). OsloCTM3 treats tropospheric and stratospheric chemistry, as well as modules for
93   carbonaceous, secondary organic, sulfate, ammonium-nitrate, sea salt and dust aerosols. Aerosols are
94   scavenged by convective and large-scale rain (ice and liquid phase), with rainfall calculated from
95   ECMWF data for convective activity, cloud fraction, and rainfall. Dry deposition applies prescribed
96   deposition velocities for different land cover types. For further details we refer to Lund et al. (2018) and
97   Søvde et al. (2012).

98   The aerosol optical depth (AOD) and instantaneous top-of-atmosphere radiative forcing due to aerosol-
99   radiation interactions (RFari) is calculated offline using a multi-stream model with the discrete ordinate
100 method DISORT (Myhre et al., 2013; Stamnes et al., 1988). The same radiative transfer model is also
101 used to estimate the radiative forcing of aerosol-cloud interactions (RFaci) (earlier denoted the cloud
102 albedo effect or Twomey effect). To account for the change in cloud droplet concentration resulting
103 from anthropogenic aerosols, which alter the cloud effective radius and thus the optical properties of the
104 clouds, the approach from Quaas et al. (2006) is used.

105 Modeled AOD is compared with retrievals from the MODIS instrument on the Aqua satellite, which is
106 available for the period 2003-2020 (MOD08, 2018). We use the combined Dark Target and Deep Blue
107 AOD at 550nm, release MOD08_M3_V6.1, downloaded from the NASA Giovanni interface. MODIS-
108 Terra AOD is also available for the same period and, for most years, is around 10% lower than MODIS-
109 Aqua on global average. However, based on previous evaluation of the MODIS AOD and a reported
110 drift in the Terra data (Levy et al., 2010; Sherman et al., 2017), we chose to use MODIS-Aqua for the
111 model comparison in the current study. We also compare modeled AOD with ground-based
112 measurements from the AERONET (AErosol RObotic NETwork) (Holben et al., 1998) Version 3 Level
113 2.0 retrievals at 500 nm. The comparison uses all available data from all months and stations for a given
114 year, with modeled AOD linearly interpolated to the latitude and longitude of each station. Temporal
115 trends in simulated and observed AOD are estimated on global-mean and grid point basis by linear least
116 square fitting and defined as statistically significant (from no trend) when the linear Pearsons correlation
117 coefficient is significant at the 0.05 level. Interannual variability is estimated on a grid point basis as the
118 standard deviation of the residual when subtracting a 10-year boxcar average (with mirrored data around
119 the end points).
120
121 Two sets of time slice simulations are performed using anthropogenic emissions from the CEDS version
122 2021 (O'Rourke et al., 2021) (hereafter "CEDS21") and ECLIPSEv6b baseline (hereafter "ECLv6")
123 inventories. The ECLv6 emissions are developed with the Greenhouse Gas - Air Pollution Interactions
124 and Synergies (GAINS) model (Amann et al., 2011). Version 6b (IIASA, 2022) consists of gridded
125 aerosol and reactive gas emissions in 5-year intervals over the period 1990-2015, as well as emissions
126 for 2008, 2009, 2014 and 2016. The Community Emission Data System (CEDS) inventory provides a
127 gridded inventory of anthropogenic greenhouse gas, reactive gases and aerosols since 1750 (Hoesly et
128 al., 2018). In the first release, the most recent year was 2014, while the 2021 release covers the period
129 until 2019. Simulations with OsloCTM3 are performed for 1990, 1995, 2000, 2005, 2010, 2014 and
130 2016 emissions, as well as years 2018 and 2019 for CEDS21. Results from the current study are
131 compared with previously published results from simulations performed with the first release of the
132 CEDS emissions (hereafter "CEDS") and three of the SSP scenarios (Lund et al., 2018; Lund et al.,
133 2019). Keeping in line with the experimental design in Lund et al. (2018), we use year 2010
134 meteorological data and each simulation is run for one year, with 6 months spin-up. In all simulations,
135 biomass burning emissions from van Marle et al. (2017) are used for the 1990-2014 period, with Global
136 Fire Emissions Database version 4 (GFED4, Randerson et al. (2017)) thereafter. We note that van Marle

137 et al. (2017) emissions are also based on GFED. Other natural emissions are fixed at the year 2010
138 levels.

140 Additionally, we use output from a timeseries of OsloCTM3 simulations with CEDS emissions and
141 actual, running meteorology covering the period 1990-2017 (the last three years uses Shared
142 Socioeconomic Pathways (SSP) 2-4.5 emissions (Fricko et al., 2017) linearly interpolated between 2015
143 and 2020) (hereafter "CEDSmet"). Originally performed for the phase III of the Aerocom project (e.g.
144 Gliß et al., 2021), this time series allows an assessment of the role of meteorology in the simulated
145 aerosol trends. Finally, we produce an updated version of this timeseries using the 2021 release of the
146 CEDS emissions for the 2001-2017 period (i.e. when the differences are most pronounced) (hereafter
147 "CEDS21met"). A summary of the experiments is provided in Table S1.

149 Figure 1 shows global, total emissions of SO_2, BC, OC and NOx over the 1990-2019 period in the three
150 inventories used here. The differences are particularly pronounced after 2005. Both ECLv6 and CEDS21
151 show substantially lower emissions of all species during this period, relative to CEDS. The largest
152 differences are for BC and OC, where CEDS21 is 20-30% lower than CEDS in 2014. For SO_2 and NOx,
153 the corresponding number is approx. 10%. ECLv6 is generally lower than both CEDS inventories,
154 particularly for SO_2, where ECLv6 is 30% lower than CEDS. While not used in this study, we also note
155 that similar differences have also been found between CEDS and two other recent global inventories,
156 the Emissions Database for Global Atmospheric Research (EDGAR) version 5 (Crippa et al., 2020) and
157 Hemispheric Transport of Air Pollution (HTAP) version 3 (Crippa et al., 2022). Important geographical
158 distinctions underlie these global differences, as demonstrated for SO_2 emissions in 2014 in Fig. 1, where
159 lower emissions in ECLv6 and CEDS21 are primarily found in China, India, and the Arabian Peninsula.
160 For many regions and species, differences exist also prior to 2014 (Fig. S1). For instance, CEDS21 has
161 the highest BC emissions in China of the three inventories until year 2000, while ECLv6 BC emissions
162 are higher than CEDS21 in both India and Africa South of the Sahara. In India, CEDS and CEDS21
163 show increasing SO_2 emissions while in ECLv6 these appear to be leveling off during 2014-2016. Aside
164 from East and South Asia, the overall temporal evolution is generally similar in the main source regions
165 across inventories, although magnitudes differ.

3 Results and discussion

170 Here we first document the differences and trends in aerosol distributions simulated with the three
171 different emission inventories, discussing burdens of individual species before focusing on total AOD.
172 We then present updated estimates of radiative forcing relative to 1990. Finally, we compare the
173 simulated global and regional AOD with observations over the period.

3.1 Aerosol burdens

176 The differences between inventories are substantial enough to influence simulated aerosol burdens
177 (column integrated aerosol mass, in mg m^{-2}) at the global mean level. For 2014, we estimate 4% and 6%
178 lower global mean burdens of BC with CEDS21 and ECLv6 (increasing to 6% and 11% when
179 considering only fossil fuel and biofuel emissions), respectively, compared to CEDS (see Table S2 for
180 absolute numbers). For primary organic aerosol (POA), the corresponding numbers are 11% and 14%
181 (30% and 40%), while global mean total sulfate burden is 8% and 15% lower. Smaller reductions are
182 also seen in the global mean secondary organic aerosol (SOA) burden. Biogenic volatile organic

Atmospheric
Chemistry
and Physics
Discussions

Open Access

EGU

183   compound (VOC) emissions, the main source of SOA, are the same in all simulations. However, the
184   SOA abundance is affected by differences in anthropogenic VOCs and by changes in primary organic
185   aerosols, which serve as substrates for SOA formation.

186   Regionally, even larger difference between the two new inventories and CEDS arise, as shown in Fig.
187   2 (see Fig. S2 for corresponding percentage changes). For all main anthropogenic aerosol species, the
188   absolute differences are consistently largest over East Asia, followed by South Asia, and larger for
189   ECLv6 than for CEDS21. Averaged over these regions, we find reductions in the year 2014 burdens of
190   BC, POA and sulfate of up to 0.45, 3.5, and 1.9 mg m^{-2}, respectively, when switching from CEDS to
191   ECLv6 (Fig. 2). This constitutes changes of around 30-40% (Fig. S2). For BC and sulfate, burdens are
192   also notably lower over North Africa and the Middle East with ECLv6 compared to both CEDS and
193   CEDS21.

194   The only species that is more abundant globally with the two new inventories, is nitrate. However, there
195   are important regional differences, where the burden is lower compared to CEDS in South Asia and on
196   the US east coast but higher in the US Midwest, parts of Africa and South America, and, especially,
197   over East Asia (Fig.2, Fig.S2). The net effect is a 15 and 24% higher global mean nitrate burden with
198   CEDS21 and ECLv6, respectively, relative to CEDS. Changes in the atmospheric nitrate distribution
199   results from a complex interplay between differences in emissions of NOx, ammonia, and SO$_2$. For
200   instance, in China (and elsewhere), the lower emissions of SO$_2$ in both ECLv6 and CEDS21 reduces the
201   chemical competition for available sulfate and, in turn, increases the production of nitrate aerosol. The
202   potential for an increasing relative role of nitrate in a world with concurrent declines in SO$_2$ emissions
203   has also been discussed in previous studies (e.g. Bauer et al., 2007; Bellouin et al., 2011).

204   Both globally and regionally, the spread in estimated aerosol load in 2014 between simulations with
205   different inventories is on the same order of magnitude or larger than the change over the 5-year period
206   from 2014 to 2019 in CEDS21. We note that regional burdens can be influenced by long-range transport
207   and thus affected by remote emission inventory differences. We also note that we find differences in
208   surface concentrations between simulations that broadly track the results for burden. While beyond the
209   scope of the present study, this may have implications for assessments of air pollution related health
210   impacts.

211

212

3.2 Aerosol optical depth

214   The differences between inventories are also directly reflected in the simulated total AOD. Over the
215   whole period considered, global mean AOD is highest in simulations with the first release of the CEDS
216   emissions, followed by CEDS21 and then ECLv6, with increasing divergence over time, especially after
217   2005 (Fig. 3a). Averaged globally, we estimate 3% and 6% lower AOD with CEDS21 and ECLv6,
218   respectively, compared to CEDS in 2014. Regional differences are larger and, as expected, most
219   pronounced over China and India (Fig. 3b). Averaged over each of these regions (indicated by the boxes
220   in Fig.3b), we estimate 20% and 30% lower AOD using the two new emission inventories, respectively,
221   in 2014. For context, we also show the interannual variability in AOD from MODIS-Aqua (see Sect. 2):
222   For most of these regions the differences between inventories are markedly larger.

223   Also plotted in Fig. 3a is the linear trend from 2005 to 2017 for each of the global timeseries. We
224   estimate that anthropogenic emission changes in the CEDS21 and ECLv6 inventories have resulted in a
225   significant (at the 0.05 level - see Sect. 2) negative linear trend in global mean AOD of -0.005 and -
226   0.006 per decade, respectively. This trend strengthens when extended to 2019 in CEDS21. A negative
227   global trend is also found when using the first CEDS release, however, it is smaller and not significant
228   over the period 2005-2014. Extending the timeseries to 2017 by assuming that emissions follow SSP2-
229   4.5 after 2014 (dashed orange line), the negative trends strengthens and switches to significant as per

230 our definition, but it remains smaller than for the other two inventories (at -0.003 per decade). We note
231 that despite the negative long-term trend and continued decrease in anthropogenic emissions, CEDS21
232 AOD is up in 2019 compared to 2018. We attribute this primarily to the high 2019 biomass burning
233 emissions in GFEDv4, more than 25% higher than in 2018.

234 Regionally, all three emission inventories result in a significant decline in AOD over the Eastern US,
235 Europe, and parts of Russia and Eurasia over the 2005-2017 period in our simulations (Fig. 3c). There
236 is also a marked negative trend over South America, as well as a weaker decline over Equatorial Africa.
237 In contrast, increases in simulated AOD are seen over Eastern Siberia. A positive, but weaker and not
238 significant at the 0.05 level, trend is also seen over Canada. This is presumably due to higher biomass
239 burning activity, which is supported by a significant increasing trend in annual biomass burning carbon
240 emissions in GFEDv4 in the boreal North America and eastern Eurasia regions over the same period
241 (not shown). There is also a decline in GFEDv4 carbon emissions in South America and Africa south of
242 the Sahara, suggesting that biomass burning is also a key driver of the simulated AOD trends there.
243 While the three inventories largely agree in all of above regions, the key differences arise, as expected,
244 when looking at Asia. Both CEDS21 and ECLv6 show a significant decreasing trend over China. A
245 decline is also present in the simulations with CEDS – when extending the time series to 2017 using
246 SSP245 emissions – but is much weaker and not significant. Real world emissions have hence likely
247 tracked well below the SSP245 projections in the region. While all three inventories show a significant
248 positive trend in AOD over India, this is strongest in CEDS. Regional trends and differences will be
249 further discussed in Sect. 3.4, including a comparison with observations.

250

3.3 Radiative forcing of anthropogenic aerosol since 1990

252 Figure 4a shows the RFari, RFaci, and net aerosol radiative forcing (RFnet, RFari plus RFaci) relative
253 to 1990 for the three sets of experiments. The net RF of changes in anthropogenic (and biomass burning)
254 aerosol is positive since 1990, except for 1995 and 2005, where a small negative forcing is estimated.
255 As shown in Fig. 1, all inventories show an increase in anthropogenic SO_2 emissions in 2005 compared
256 to the years before, and both these years have relatively high biomass burning emissions in these years.
257 This positive global mean RF is determined by the balance between a positive forcing over the northern
258 extratropics, predominantly due to aerosol-radiation interactions, and a negative forcing over Asia and
259 parts of South America and Africa (Fig. S3).

260 In 2014, we estimate a global mean RFnet of 0.03 W m^{-2} for CEDS, 0.08 W m^{-2} for CEDS21, and 0.12
261 W m^{-2} for ECLv6 relative to 1990, of which the RFari constitutes 0.07 W m^{-2}, 0.09 W m^{-2} and 0.10 W
262 m^{-2}. Our CEDS RFari estimate is similar to the multi-model mean RFari of 0.05 W m^{-2} derived for the
263 1990-2015 period using ECLIPSE version 5 emissions by Myhre et al. (2017). The same study estimated
264 a model mean RFnet of 0.1 W m^{-2}, but with a significant intermodel spread, from close to zero to more
265 than 0.2 W m^{-2}. This spread is larger than the difference between estimates with different inventories in
266 the present analysis. Nevertheless, the differences in emissions between CEDS and CEDS21 (ECLv6)
267 translates to a factor 3 (5) stronger RFnet in our calculations. These differences arise primarily from the
268 weaker forcing over East Asia and, for ECLv6, also over South Asia and South and Central America,
269 compared to CEDS (Figure 4b). In contrast, all three inventories give similar RF over the 1990-2014
270 period in North America, Europe, and Eurasia and show the effect of the southeastward shift in
271 emissions over the past decades. A negative forcing is seen over China during this period with all three
272 inventories; however, this is markedly weaker in CEDS21 and ECLv6 (Fig. S3).

273 Figure 4c shows the RFnet in 2019 relative to 2014, i.e. the five most recent years provided by CEDS21.
274 In contrast to the 1990-2014 period (Fig. S3), a net positive forcing is estimated over China, in line with
275 the decline in SO_2 emissions. Over India, the forcing has remained negative, although weaker than
276 during the preceding period. Over Europe and western Russia, the bulk of the emission decline, and

277 hence forcing, was already realized until 2014, with only relatively weaker RF seen until 2019. On
278 global average, RFnet is estimated to be 0.10 W m^{-2} in 2019 relative to 1990 for CEDS21 emissions
279 (small reduction from 0.13 W m^{-2} in 2018 likely due to stronger biomass burning emissions in 2019)
280 (Fig. 4a).

281 In the first CEDS release, the most recent historical year was 2014. Using a selection of the SSP
282 scenarios, Lund et al. (2019) quantified the projected aerosol-induced RF. The orange hatched bars in
283 Fig. 4 show the range in RFnet in 2020 and 2030 (relative to 1990) estimated with SSP1-1.9, SSP2-4.5
284 and SSP3-7.0 in that study. The RFnet in 2019 estimated with CEDS21 is close to the lower end of the
285 bar, i.e. the RFnet projected under SSP3-7.0. However, prior to this higher biomass burning year, there
286 are indications that the RFnet from simulations with CEDS21 tracked closer to SSP2-4.5 or an even
287 lower emission pathway.

288 The dipole pattern of aerosol changes and resulting RF over India versus China was first highlighted by
289 Samset et al. (2019). Using emissions from CEDS and SSP1-1.9, SSP2-4.5 and SSP3-7.0, combined
290 with a radiative kernel approach, that study estimated a range of 2014-2030 aerosol (SO$_2$ and BC) RF
291 of -1.0 W m^{-2} (SSP1-1.9) to 0.82 W m^{-2} (SSP2-4.5) over India, and 0.06 W m^{-2} (SSP2-4.5) to 1.10 W
292 m^{-2} (SSP3-7.0) over China. Part of this range can be attributed to poor knowledge of current, and hence
293 also future, regional emissions (Samset et al. 2019). In the present study, we estimate regionally
294 averaged RFnet in 2019 relative to 2014 of -0.09 W m^{-2} and 0.22 W m^{-2} over India and China,
295 respectively. For China, this recent RFnet is about 20% of the previously estimated difference between
296 high and low future aerosol emission scenarios in 2030 (SSP2-4.5 and SSP3-7.0). Uncertainties in the
297 amount of recent emission reductions can therefore markedly affect assessments of projected near-tern
298 aerosol-induced climate impacts, as they depend on a well constrained starting point.

299

300 **3.4 Comparison with observed aerosol trends**

301 We have demonstrated that the differences between recent global inventories translates to notable
302 differences in global and regional anthropogenic aerosol distributions, trends, and radiative forcing. To
303 assess whether the model captures observed trends better with the CEDS21 emissions, we compare
304 simulated AOD to MODIS-Aqua retrievals and ground-based AERONET measurement. For this
305 evaluation, simulations where the model is driven by meteorology for the respective years, referred to
306 as CEDSmet and CEDS21met, are used (see Sect. 2). Figure 5a shows the annual, global mean simulated
307 AOD from 1990 to 2017 and the MODIS-Aqua AOD from 2003 to 2019. Dashed lines show the linear
308 2005-2017 trends. Figures 5b-d show the spatially explicit trends.

309 The simulated global mean AOD is lower than the MODIS-Aqua, by around 20%. However, the overall
310 geographical pattern of the observed AOD is captured by the model (Fig. S4). Furthermore, the AOD
311 simulated by the OsloCTM3 is within, although in the lower range, of the spread in AOD between the
312 CMIP and AeroCom models (Vogel et al., 2022). As also shown by Vogel et al. (2022), there can be a
313 notable spread also in AOD derived from different satellite products, where MODIS retrievals comes
314 out in the upper end. The OsloCTM3 AOD is within the standard deviation range of satellite derived
315 AOD found in that study. Overall, this suggests a reasonable OsloCTM3 performance in terms of
316 magnitude and distribution.

317 In terms of temporal evolution, we estimate weakly negative linear trends in simulated global mean
318 AOD from 2005 to 2017 with both CEDS and CEDS21, albeit not significant at the 0.05 level. Using
319 the original release of the CEDS emissions with the SSP2-4.5 extension (i.e. CEDSmet), we calculate a
320 trend in global mean AOD of -0.001 per decade. With CEDS21 emissions, this strengthens to -0.003
321 per decade. These are weaker than the trends associated with anthropogenic emission changes derived
322 from the fixed meteorology simulations in Sect. 3.1 (-0.003 and -0.005 per decade with CEDS and
323 CEDS21, respectively) and not significant, demonstrating the influence of variability in meteorology

324 and natural aerosols. Consistent evidence of a declining influence of anthropogenic aerosols on climate
325 has also been found for a range of observed variables (Quaas et al., 2022).

326 In contrast, MODIS-Aqua suggests a positive linear trend of 0.001 per decade in global mean AOD over
327 the 2005-2017 period, further strengthening to 0.004 per decade when considering the full time series
328 of available observations (2003-2019). A positive global AOD trend was also found in ground based
329 observations by Mortier et al. (2020). This positive observed trend is driven by an increase in AOD over
330 oceans, associated with sea salt aerosol, as well as over boreal regions in the northern high latitudes,
331 associated with biomass burning aerosol (Fig. 5b). We do not, however, find this trend to be significant
332 at the 0.05 level. This could in part be due to influence from the substantial year-to-year variability seen
333 after 2010, which was also pointed out by Vogel et al. (2022). While we are primarily focused on the
334 anthropogenically-influenced regions in the present analysis, we note that the model does not fully
335 capture the trends over high-latitude boreal biomass burning regions, nor over the Southern hemisphere
336 oceanic regions (Fig. 5c-d). While studies to date show a wide spread in simulated response of sea spray
337 aerosol to changing climate, recent studies have suggested increases both at the global (Struthers et al.,
338 2013) and, even more strongly, at the regional scale (Korhonen et al., 2010). Moreover, other factors
339 than wind speed are proposed to be possible drivers of a climate feedback on sea salt aerosol (e.g. Paulot
340 et al., 2020, and references therein). Better understanding of changing natural aerosols in the OsloCTM3
341 and reasons for the discrepancies compared to observations require further, dedicated studies.

342 Regionally, there are significant observed declines in AOD over East Asia, eastern US, and parts of
343 Europe (Fig. 5b). A negative trend is also seen over South America; however, this is not significantly
344 different from zero over this period. A significant positive trend is seen over India. The trends over
345 North America, Europe, and Asia are consistent with the concurrent changes in anthropogenic emissions
346 and have been seen in both ground based and remote observations of both AOD and other variables (Gui
347 et al., 2021; Moseid et al., 2020; Paulot et al., 2018; Quaas et al., 2022). The trends in AOD simulated
348 with the OsloCTM3 show the same sign as MODIS-Aqua in most regions, for both emission inventories
349 (Fig. 5c-d). As expected from results in preceding sections, the main differences, between CEDSmet
350 and MODIS-Aqua, as well as between model results, arise over Asia. We therefore take a closer look at
351 the evolution of AOD in this region (Fig. 6). Both MODIS-Aqua and the OsloCTM3 show an increase
352 in AOD over India from 2008, although modeled changes are weaker in magnitude. As indicated by
353 preceding sections, using CEDS21 results in marked improvements compared to observed AOD trends
354 over China, both for the first and last full 5-year periods. A continuation of the dipole pattern of increases
355 and decreases over India and China is evident from the observations for the 2018-2020 period (noting
356 that the COVID-19 pandemic resulted in significant temporary impacts on emissions in 2020). In the
357 case of India, this increase suggests that the leveling off in anthropogenic emissions in the inventories
358 (Fig. S1) may not be representative of the observed evolution. However, we note that natural emissions,
359 as well as long-range transport, may factor into the observed trend as well, complicating the comparison.
360 We also note that the 5-year deviations exhibit quite some variability over the Middle East, with both
361 positive and negative deviations from the baseline period. While anthropogenic emissions in this region
362 increase steadily over the period (by 13-40% depending on species) in the inventories used in the present
363 study, the strong influence from dust emissions in this region likely contributes to the temporal
364 variability.

365 A previous OsloCTM3 study by Lund et al. (2018) found an improved agreement between year 2010
366 ground-based observations and model output, including over Asia, when switching from CMIP5 and
367 ECLIPSEv5 emissions to CEDS, the latter having higher emissions. This seemingly contradicts
368 expectations following the now-known biases in this first release of CEDS. Here we repeat the
369 comparison with AERONET measurements, but for year 2014. Resulting scatter density plots are given
370 in the SI.

371 On global average, the model underestimates observed AOD, consistent with the comparison against
372 MODIS-Aqua and Lund et al. (2018). The normalized mean bias (NMB) ranges from 22 to 29% in the

373   simulations with fixed meteorology (Fig. S5). This underestimation is somewhat larger than what was
374   found by Lund et al. (2018), but since the year, number of measurements and stations are different, a
375   direct comparison is difficult. These simulations use 2010 meteorology, however, the difference in
376   meteorology appears to only explain a small part of the bias, as can be seen by comparing scatter density
377   plots for CEDS and CEDSmet and CEDS21 and CEDS21met. Interannual variability may also play a
378   role. We consistently find higher NMB and lower correlation when switching from the original CEDS
379   release to CEDS21 and ECLv6. The largest normalized mean bias (NMB) of -29% is found in the
380   simulation using ECLv6 emissions, the lowest of the three inventories, while the smallest NMB is
381   calculated for CEDS (-22%) (Fig. S5). Hence, while the model is better able to represent observed recent
382   aerosol trends over East Asia with newer emission inventories, results point to other issues. Specifically,
383   our analysis indicates that the too high emissions in CEDS may have partly concealed underestimations
384   of other aerosol sources in the model. One possible candidate is dust aerosol from soils in agricultural
385   regions and human activities in urban areas (e.g. construction, non-exhaust transport emissions), which
386   are suggested to give an important contribution to the particulate matter load (e.g. Chen et al., 2019; Xia
387   et al., 2022), but is stilling missing from many global models, including the OsloCTM3.

388

389   4 Conclusions

390   We have investigated the impact of differences between recent global emission inventories on simulated
391   anthropogenic aerosol abundances, and associated radiative forcing, from 1990 to 2019. Simulations
392   with the chemical transport model OsloCTM3 and the CEDS emission inventory, developed for the
393   sixth cycle of the IPCC, are compared with corresponding results using two newer inventories: The
394   CEDS 2021 update (CEDS21) and the ECLIPSE version 6b (ECLv6). Our main objective was to explore
395   the implications of now known biases in CEDS, specifically the underestimation of the decline in
396   Chinese precursor emissions and an overestimation of Asian and African BC and OC emissions. While
397   largely addressed in the updated release, these biases introduce added uncertainty in recently published
398   estimates of the anthropogenic aerosol evolution and effects.

399   We have found that, apart for nitrate, the CEDS21 (ECLv6) result in lower global aerosol burdens than
400   CEDS, ranging from 4% (6%) for BC to approx. 10% (15%) for sulfate and POA in 2014 (the most
401   recent historical year common for all scenarios). Differences are consistently most pronounced over
402   East Asia, followed by South Asia, where they are on the order of 30-60% depending on species and
403   scenario. We also note marked differences between CEDS and ECLv6 over North Africa and the Middle
404   East. In our model, the global mean fine mode nitrate burden is 15% (24%) higher with CEDS21
405   (ECLv6) relative to CEDS, but with regional heterogeneity in sign of the difference. Overall, we
406   estimate 3% (6%) lower total AOD with CEDS21 (ECLv6), respectively, compared to CEDS in 2014.
407   The difference reaches approx. 20% and 30% over East and South Asia.

408   Changes in anthropogenic emissions result in a negative linear trend in global mean AOD over the 2005-
409   2017 period with all three inventories, but increasingly stronger with CEDS21 (ECLv6). Importantly,
410   we find that the model is better able to capture the declining AOD trend observed by MODIS-Aqua over
411   China with both new inventories, whereas it is weak and not significant with CEDS. A positive AOD
412   trend is found over India; however, it is weaker in the model than in MODIS-Aqua data.

413   Using offline radiative transfer calculations, we estimate a global mean net aerosol RF in 2014 relative
414   to 1990 of 0.03 W m^{-2} for CEDS, 0.08 W m^{-2} for CEDS21, and 0.12 W m^{-2} for ECLv6. Following the
415   continued declined in CEDS21 emissions, a positive global-mean net RF is also estimated for the 5-year
416   period 2014-2019, with the strongest positive signals over China and easter US.

417   While the focus of the present study is on anthropogenic aerosols, our comparison with observed AOD
418   reveals potential issues related to the representation of natural aerosols in the OsloCTM3. Specifically,
419   the modeled AOD does not capture the slight positive global trend apparent in MODIS-Aqua, with key

discrepancies over northern hemisphere biomass burning regions and the Southern Ocean. For individual years, we also find a larger underestimation in AOD compared to AERONET measurements when switching from CEDS to the lower CEDS21 and ECLv6 emissions, despite better representation of some key regional trends. This could indicate that too high anthropogenic emission estimates have masked challenges with for instance dust emissions. Dedicated studies are required to investigate this in more detail.

Anthropogenic aerosols are changing rapidly, particularly in Asia, with potentially large but insufficiently quantified implications for regional climate. We have demonstrated that differences between recent emission inventories can have marked effects on the magnitude and trend of regional and global aerosol abundances, and in turn on estimates of radiative forcing. Although additional studies are required to fully quantify the broader implications for aerosol-induced climate and health impacts, our results facilitate comparisons between existing and upcoming studies, using different emission inventories, of anthropogenic aerosols and their effects.

Code availability

The OsloCTM3 is available on from https://github.com/NordicESMhub/OsloCTM3.

Data availability

Model data underlying the manuscript figures are available from 10.6084/m9.figshare.20254764. AERONET data is downloaded from https://aeronet.gsfc.nasa.gov/, MODIS data from https://giovanni.gsfc.nasa.gov/giovanni/, and CEDS21 emissions from the PNNL DataHub https://doi.org/10.25584/PNNLDataHub/1779095.

Author contributions

MTL led the study design and analysis and the writing. The OsloCTM3 model experiments were performed by MTL and RBS. GM performed the radiative transfer modeling and BHS contributed graphics, silly jokes, and MODIS analysis. All authors contributed to the discussions and writing.

Competing interests

The authors declare that they have no conflict of interest.

458   **References**

459   Bauer S. E., Koch D., Unger N., Metzger S. M., Shindell D. T. & Streets D. G. Nitrate
460   aerosols today and in 2030: a global simulation including aerosols and tropospheric ozone,
461   *Atmospheric Chemistry and Physics.* 7(19), 5043-5059, 2007.
462   Bauer S. E., Tsigaridis K., Faluvegi G., Kelley M., Lo K. K., Miller R. L., Nazarenko L.,
463   Schmidt G. A. & Wu J. Historical (1850–2014) Aerosol Evolution and Role on Climate Forcing Using
464   the GISS ModelE2.1 Contribution to CMIP6, *Journal of Advances in Modeling Earth Systems.* 12(8),
465   e2019MS001978, https://doi.org/10.1029/2019MS001978, 2020.
466   Bellouin N., Rae J., Jones A., Johnson C., Haywood J. & Boucher O. Aerosol forcing in the
467   Climate Model Intercomparison Project (CMIP5) simulations by HadGEM2-ES and the role of
468   ammonium nitrate, *Journal of Geophysical Research-Atmospheres.* 116, D20206,
469   10.1029/2011jd016074, 2011.
470   Chen S., Zhang X., Lin J., Huang J., Zhao D., Yuan T., Huang K., Luo Y., Jia Z., Zang Z., Qiu
471   Y. a. & Xie L. Fugitive Road Dust PM2.5 Emissions and Their Potential Health Impacts,
472   *Environmental Science & Technology.* 53(14), 8455-8465, 10.1021/acs.est.9b00666, 2019.
473   Cheng J., Tong D., Liu Y., Yu S., Yan L., Zheng B., Geng G., He K. & Zhang Q. Comparison
474   of Current and Future PM2.5 Air Quality in China Under CMIP6 and DPEC Emission Scenarios,
475   *Geophysical Research Letters.* 48(11), e2021GL093197, https://doi.org/10.1029/2021GL093197,
476   2021.
477   Cherian R. & Quaas J. Trends in AOD, Clouds, and Cloud Radiative Effects in Satellite Data
478   and CMIP5 and CMIP6 Model Simulations Over Aerosol Source Regions, *Geophysical Research
479   Letters.* 47(9), e2020GL087132, https://doi.org/10.1029/2020GL087132, 2020.
480   Chowdhury S., Pozzer A., Haines A., Klingmüller K., Münzel T., Paasonen P., Sharma A.,
481   Venkataraman C. & Lelieveld J. Global health burden of ambient PM2.5 and the contribution of
482   anthropogenic black carbon and organic aerosols, *Environment International.* 159, 107020,
483   https://doi.org/10.1016/j.envint.2021.107020, 2022.
484   Crippa M., Guizzardi D., Muntean M., Schaaf E., Dentener F., van Aardenne J. A., Monni S.,
485   Doering U., Olivier J. G. J., Pagliari V. & Janssens-Maenhout G. Gridded emissions of air pollutants
486   for the period 1970–2012 within EDGAR v4.3.2, *Earth Syst. Sci. Data.* 10(4), 1987-2013,
487   10.5194/essd-10-1987-2018, 2018.
488   Crippa M., Solazzo E., Huang G., Guizzardi D., Koffi E., Muntean M., Schieberle C.,
489   Friedrich R. & Janssens-Maenhout G. High resolution temporal profiles in the Emissions Database for
490   Global Atmospheric Research, *Scientific Data.* 7(1), 121, 10.1038/s41597-020-0462-2, 2020.
491   Crippa M., Guizzardi D., Butler T., Keating T., Kaminski J., Kuenen, J. , Kurokawa J., Satoru
492   C., Pouliot G., Racine J., Moran M., Klimont Z., Wu R., Manseau P., Barron H., Smith S., Muntean
493   M., Solazzo E., Banja M., Schaaf E., Pagani F., Monforti F. & Pisoni E. HTAPv3 emission mosaic: a
494   global effort to tackle air quality issues, in preparation., 2022.
495   Elguindi N., Granier C., Stavrakou T., Darras S., Bauwens M., Cao H., Chen C., Denier van
496   der Gon H. A. C., Dubovik O., Fu T. M., Henze D. K., Jiang Z., Keita S., Kuenen J. J. P., Kurokawa
497   J., Liousse C., Miyazaki K., Müller J.-F., Qu Z., Solmon F. & Zheng B. Intercomparison of
498   Magnitudes and Trends in Anthropogenic Surface Emissions From Bottom-Up Inventories, Top-
499   Down Estimates, and Emission Scenarios, *Earth's Future.* 8(8), e2020EF001520,
500   https://doi.org/10.1029/2020EF001520, 2020.
501   Forster P., Storelvmo T., Armour K., Collins W., Dufresne J.-L., Frame D., Lunt D. J.,
502   Mauritsen T., Palmer M. D., Watanabe M., Wild M. & Zhang H. The Earth's Energy Budget, Climate
503   Feedbacks, and Climate Sensitivity. In Climate Change 2021: The Physical Science Basis.
504   Contribution of Working Group I to the Sixth Assessment Report of the Intergovernmental Panel on
505   Climate Change [Masson-Delmotte, V., P. Zhai, A. Pirani, S.L. Connors, C. Péan, S. Berger, N. Caud,
506   Y. Chen, L. Goldfarb, M.I. Gomis, M. Huang, K. Leitzell, E. Lonnoy, J.B.R. Matthews, T.K.
507   Maycock, T. Waterfield, O. Yelekçi, R. Yu, and B. Zhou (eds.)]. Cambridge University Press,
508   Cambridge, United Kingdom and New York, NY, USA, pp. 923–1054,
509   doi:10.1017/9781009157896.009.

510   , 2021.

511   Fricko O., Havlik P., Rogelj J., Klimont Z., Gusti M., Johnson N., Kolp P., Strubegger M.,
512   Valin H., Amann M., Ermolieva T., Forsell N., Herrero M., Heyes C., Kindermann G., Krey V.,
513   McCollum D. L., Obersteiner M., Pachauri S., Rao S., Schmid E., Schoepp W. & Riahi K. The marker
514   quantification of the Shared Socioeconomic Pathway 2: A middle-of-the-road scenario for the 21st
515   century, *Global Environmental Change.* 42, 251-267,
516   https://doi.org/10.1016/j.gloenvcha.2016.06.004, 2017.
517   Gliß J., Mortier A., Schulz M., Andrews E., Balkanski Y., Bauer S. E., Benedictow A. M. K.,
518   Bian H., Checa-Garcia R., Chin M., Ginoux P., Griesfeller J. J., Heckel A., Kipling Z., Kirkevåg A.,
519   Kokkola H., Laj P., Le Sager P., Lund M. T., Lund Myhre C., Matsui H., Myhre G., Neubauer D., van
520   Noije T., North P., Olivié D. J. L., Rémy S., Sogacheva L., Takemura T., Tsigaridis K. & Tsyro S. G.
521   AeroCom phase III multi-model evaluation of the aerosol life cycle and optical properties using
522   ground- and space-based remote sensing as well as surface in situ observations, *Atmos. Chem. Phys.*
523   21(1), 87-128, 10.5194/acp-21-87-2021, 2021.
524   Gui K., Che H., Wang Y., Xia X., Holben B. N., Goloub P., Cuevas-Agulló E., Yao W.,
525   Zheng Y., Zhao H., Li L. & Zhang X. A global-scale analysis of the MISR Level-3 aerosol optical
526   depth (AOD) product: Comparison with multi-platform AOD data sources, *Atmospheric Pollution
527   Research.* 12(12), 101238, https://doi.org/10.1016/j.apr.2021.101238, 2021.
528   Hoesly R. M., Smith S. J., Feng L., Klimont Z., Janssens-Maenhout G., Pitkanen T., Seibert J.
529   J., Vu L., Andres R. J., Bolt R. M., Bond T. C., Dawidowski L., Kholod N., Kurokawa J. I., Li M., Liu
530   L., Lu Z., Moura M. C. P., O'Rourke P. R. & Zhang Q. Historical (1750–2014) anthropogenic
531   emissions of reactive gases and aerosols from the Community Emission Data System (CEDS), *Geosci.
532   Model Dev.* 2018(11), 369-408, https://doi.org/10.5194/gmd-11-369-2018, 2018.
533   Holben B. N., Eck T. F., Slutsker I., Tanré D., Buis J. P., Setzer A., Vermote E., Reagan J. A.,
534   Kaufman Y. J., Nakajima T., Lavenu F., Jankowiak I. & Smirnov A. AERONET—A Federated
535   Instrument Network and Data Archive for Aerosol Characterization, *Remote Sensing of Environment.*
536   66(1), 1-16, https://doi.org/10.1016/S0034-4257(98)00031-5, 1998.
537
538   Kanaya Y., Yamaji K., Miyakawa T., Taketani F., Zhu C., Choi Y., Komazaki Y., Ikeda K.,
539   Kondo Y. & Klimont Z. Rapid reduction in black carbon emissions from China: evidence from 2009–
540   2019 observations on Fukue Island, Japan, *Atmos. Chem. Phys.* 20(11), 6339-6356, 10.5194/acp-20-
541   6339-2020, 2020.
542   Klimont Z., Smith S. J. & Cofala J. The last decade of global anthropogenic sulfur dioxide:
543   2000–2011 emissions, *Environmental Research Letters.* 8(1), 014003, 10.1088/1748-
544   9326/8/1/014003, 2013.
545   Klimont Z., Kupiainen K., Heyes C., Purohit P., Cofala J., Rafaj P., Borken-Kleefeld J. &
546   Schöpp W. Global anthropogenic emissions of particulate matter including black carbon, *Atmos.
547   Chem. Phys.* 17(14), 8681-8723, 10.5194/acp-17-8681-2017, 2017.
548   Korhonen H., Carslaw K. S., Forster P. M., Mikkonen S., Gordon N. D. & Kokkola H.
549   Aerosol climate feedback due to decadal increases in Southern Hemisphere wind speeds, *Geophysical
550   Research Letters.* 37(2), https://doi.org/10.1029/2009GL041320, 2010.
551   Kurokawa J. & Ohara T. Long-term historical trends in air pollutant emissions in Asia:
552   Regional Emission inventory in ASia (REAS) version 3, *Atmos. Chem. Phys.* 20(21), 12761-12793,
553   10.5194/acp-20-12761-2020, 2020.
554   Levy R. C., Remer L. A., Kleidman R. G., Mattoo S., Ichoku C., Kahn R. & Eck T. F. Global
555   evaluation of the Collection 5 MODIS dark-target aerosol products over land, *Atmos. Chem. Phys.*
556   10(21), 10399-10420, 10.5194/acp-10-10399-2010, 2010.
557   Li C., McLinden C., Fioletov V., Krotkov N., Carn S., Joiner J., Streets D., He H., Ren X., Li
558   Z. & Dickerson R. R. India Is Overtaking China as the World's Largest Emitter of Anthropogenic
559   Sulfur Dioxide, *Scientific Reports.* 7(1), 14304, 10.1038/s41598-017-14639-8, 2017.
560   Lund M. T., Myhre G., Haslerud A. S., Skeie R. B., Griesfeller J., Platt S. M., Kumar R.,
561   Myhre C. L. & Schulz M. Concentrations and radiative forcing of anthropogenic aerosols from 1750
562   to 2014 simulated with the Oslo CTM3 and CEDS emission inventory, *Geosci. Model Dev.* 11(12),
563   4909-4931, 10.5194/gmd-11-4909-2018, 2018.

564   Lund M. T., Myhre G. & Samset B. H. Anthropogenic aerosol forcing under the Shared
565   Socioeconomic Pathways, *Atmos. Chem. Phys.* 19(22), 13827-13839, 10.5194/acp-19-13827-2019,
566   2019.
567   Lund M. T., Aamaas B., Stjern C. W., Klimont Z., Berntsen T. K. & Samset B. H. A
568   continued role of short-lived climate forcers under the Shared Socioeconomic Pathways, *Earth Syst.*
569   *Dynam.* 11(4), 977-993, 10.5194/esd-11-977-2020, 2020.
570   MOD08 MODIS Level 3 Atmosphere Products (MOD 08), Data Products Handbook Volume
571   2. https://modis.gsfc.nasa.gov/data/dataprod/dataproducts.php?MOD_NUMBER=08 (accessed
572   04/26/2018), 2018.
573   Mortier A., Gliß J., Schulz M., Aas W., Andrews E., Bian H., Chin M., Ginoux P., Hand J.,
574   Holben B., Zhang H., Kipling Z., Kirkevåg A., Laj P., Lurton T., Myhre G., Neubauer D., Olivié D.,
575   von Salzen K., Skeie R. B., Takemura T. & Tilmes S. Evaluation of climate model aerosol trends with
576   ground-based observations over the last 2 decades – an AeroCom and CMIP6 analysis, *Atmos. Chem.*
577   *Phys.* 20(21), 13355-13378, 10.5194/acp-20-13355-2020, 2020.
578   Moseid K. O., Schulz M., Storelvmo T., Julsrud I. R., Olivié D., Nabat P., Wild M., Cole J. N.
579   S., Takemura T., Oshima N., Bauer S. E. & Gastineau G. Bias in CMIP6 models as compared to
580   observed regional dimming and brightening, *Atmos. Chem. Phys.* 20(24), 16023-16040, 10.5194/acp-
581   20-16023-2020, 2020.
582   Myhre G., Samset B. H., Schulz M., Balkanski Y., Bauer S., Berntsen T. K., Bian H., Bellouin
583   N., Chin M., Diehl T., Easter R. C., Feichter J., Ghan S. J., Hauglustaine D., Iversen T., Kinne S.,
584   Kirkevåg A., Lamarque J. F., Lin G., Liu X., Lund M. T., Luo G., Ma X., van Noije T., Penner J. E.,
585   Rasch P. J., Ruiz A., Seland Ø., Skeie R. B., Stier P., Takemura T., Tsigaridis K., Wang P., Wang Z.,
586   Xu L., Yu H., Yu F., Yoon J. H., Zhang K., Zhang H. & Zhou C. Radiative forcing of the direct
587   aerosol effect from AeroCom Phase II simulations, *Atmos. Chem. Phys.* 13(4), 1853-1877,
588   10.5194/acp-13-1853-2013, 2013.
589   Myhre G., Aas W., Cherian R., Collins W., Faluvegi G., Flanner M., Forster P., Hodnebrog
590   Ø., Klimont Z., Lund M. T., Mülmenstädt J., Lund Myhre C., Olivié D., Prather M., Quaas J., Samset
591   B. H., Schnell J. L., Schulz M., Shindell D., Skeie R. B., Takemura T. & Tsyro S. Multi-model
592   simulations of aerosol and ozone radiative forcing due to anthropogenic emission changes during the
593   period 1990–2015, *Atmos. Chem. Phys.* 17(4), 2709-2720, 10.5194/acp-17-2709-2017, 2017.
594   O'Rourke P. R., Smith S. J., Mott A., Ahsan H., McDuffie E. E., Crippa M., Klimont S.,
595   McDonald B., Wang Z., Nicholson M. B., Feng L. & Hoesly R. M. (2021), CEDS v-2021-02-05
596   Emission Data 1975-2019 (Version Feb-05-2021), edited, Zenodo.
597   Paulot F., Paynter D., Ginoux P., Naik V. & Horowitz L. W. Changes in the aerosol direct
598   radiative forcing from 2001 to 2015: observational constraints and regional mechanisms, *Atmos.*
599   *Chem. Phys.* 18(17), 13265-13281, 10.5194/acp-18-13265-2018, 2018.
600   Paulot F., Paynter D., Winton M., Ginoux P., Zhao M. & Horowitz L. W. Revisiting the
601   Impact of Sea Salt on Climate Sensitivity, *Geophysical Research Letters.* 47(3), e2019GL085601,
602   https://doi.org/10.1029/2019GL085601, 2020.
603   Quaas J., Boucher O. & Lohmann U. Constraining the total aerosol indirect effect in the
604   LMDZ and ECHAM4 GCMs using MODIS satellite data, *Atmos. Chem. Phys.* 6(4), 947-955,
605   10.5194/acp-6-947-2006, 2006.
606   Quaas J., Jia H., Smith C., Albright A. L., Aas W., Bellouin N., Boucher O., Doutriaux-
607   Boucher M., Forster P. M., Grosvenor D., Jenkins S., Klimont Z., Loeb N. G., Ma X., Naik V., Paulot
608   F., Stier P., Wild M., Myhre G. & Schulz M. Robust evidence for reversal in the aerosol effective
609   climate forcing trend, *Atmos. Chem. Phys. Discuss.* 2022, 1-25, 10.5194/acp-2022-295, 2022.
610   Ramachandran S., Rupakheti M. & Cherian R. Insights into recent aerosol trends over Asia
611   from observations and CMIP6 simulations, *Science of The Total Environment.* 807, 150756,
612   https://doi.org/10.1016/j.scitotenv.2021.150756, 2022.
613   Randerson J. T., van der Werf G. R., Giglio L., Collatz G. J. & Kasibhatla P. S. Global Fire
614   Emissions Database, Version 4.1 (GFEDv4). ORNL DAAC, Oak Ridge, Tennessee, USA. ,
615   https://doi.org/10.3334/ORNLDAAC/1293, 2017.
616   Samset B. H., Lund M. T., Bollasina M., Myhre G. & Wilcox L. Emerging Asian aerosol
617   patterns, *Nature Geoscience.* 12(8), 582-584, 10.1038/s41561-019-0424-5, 2019.

618   Sherman J. P., Gupta P., Levy R. C. & Sherman P. J. An Evaluation of MODIS-Retrieved
619   Aerosol Optical Depth over a Mountainous AERONET Site in the Southeastern US, *Aerosol and Air*
620   *Quality Research.* 16(12), 3243-3255, 10.4209/aaqr.2015.09.0568, 2017.
621   Stamnes K., Tsay S. C., Wiscombe W. & Jayaweera K. Numerically stable algorithm for
622   discrete-ordinate-method radiative transfer in multiple scattering and emitting layered media, *Appl.*
623   *Opt.* 27(12), 2502-2509, 10.1364/AO.27.002502, 1988.
624   Struthers H., Ekman A. M. L., Glantz P., Iversen T., Kirkevåg A., Seland Ø., Mårtensson E.
625   M., Noone K. & Nilsson E. D. Climate-induced changes in sea salt aerosol number emissions: 1870 to
626   2100, *Journal of Geophysical Research: Atmospheres.* 118(2), 670-682,
627   https://doi.org/10.1002/jgrd.50129, 2013.
628   Su W., Liang L., Myhre G., Thorsen T. J., Loeb N. G., Schuster G. L., Ginoux P., Paulot F.,
629   Neubauer D., Checa-Garcia R., Matsui H., Tsigaridis K., Skeie R. B., Takemura T., Bauer S. E. &
630   Schulz M. Understanding Top-of-Atmosphere Flux Bias in the AeroCom Phase III Models: A Clear-
631   Sky Perspective, *Journal of Advances in Modeling Earth Systems.* 13(9), e2021MS002584,
632   https://doi.org/10.1029/2021MS002584, 2021.
633   Szopa S., Naik V., Adhikary B., Artaxo P., Berntsen T., Collins W. D., Fuzzi S., Gallardo L.,
634   Kiendler Scharr A., Klimont Z., Liao H., Unger N. & Zanis P. Short-Lived Climate Forcers. In:
635   Climate Change 2021: The Physical Science Basis. Contribution of Working Group I to the Sixth
636   Assessment Report of the Intergovernmental Panel on Climate Change [Masson-Delmotte, V., P. Zhai,
637   A. Pirani, S. L. Connors, C. Péan, S. Berger, N. Caud, Y. Chen, L. Goldfarb, M. I. Gomis, M. Huang,
638   K. Leitzell, E. Lonnoy, J. B. R. Matthews, T. K. Maycock, T. Waterfield, O. Yelekçi, R. Yu and B.
639   Zhou (eds.)]. Cambridge University Press, Cambridge, United Kingdom and New York, NY, USA,
640   pp. 817–922 doi:10.1017/9781009157896.008, 2021.
641   Søvde O. A., Prather M. J., Isaksen I. S. A., Berntsen T. K., Stordal F., Zhu X., Holmes C. D.
642   & Hsu J. The chemical transport model Oslo CTM3, *Geosci. Model Dev.* 5(6), 1441-1469,
643   10.5194/gmd-5-1441-2012, 2012.
644   Tong D., Cheng J., Liu Y., Yu S., Yan L., Hong C., Qin Y., Zhao H., Zheng Y., Geng G., Li
645   M., Liu F., Zhang Y., Zheng B., Clarke L. & Zhang Q. Dynamic projection of anthropogenic
646   emissions in China: methodology and 2015–2050 emission pathways under a range of socio-
647   economic, climate policy, and pollution control scenarios, *Atmos. Chem. Phys.* 20(9), 5729-5757,
648   10.5194/acp-20-5729-2020, 2020.
649   van Marle M. J. E., Kloster S., Magi B. I., Marlon J. R., Daniau A. L., Field R. D., Arneth A.,
650   Forrest M., Hantson S., Kehrwald N. M., Knorr W., Lasslop G., Li F., Mangeon S., Yue C., Kaiser J.
651   W. & van der Werf G. R. Historic global biomass burning emissions for CMIP6 (BB4CMIP) based on
652   merging satellite observations with proxies and fire models (1750–2015), *Geosci. Model Dev.* 10(9),
653   3329-3357, 10.5194/gmd-10-3329-2017, 2017.
654   Vogel A., Alessa G., Scheele R., Weber L., Dubovik O., North P. & Fiedler S. Uncertainty in
655   Aerosol Optical Depth From Modern Aerosol-Climate Models, Reanalyses, and Satellite Products,
656   *Journal of Geophysical Research: Atmospheres.* 127(2), e2021JD035483,
657   https://doi.org/10.1029/2021JD035483, 2022.
658   Wang C.-S., Wang Z.-L., Lei Y.-D., Zhang H., Che H.-Z. & Zhang X.-Y. Differences in East
659   Asian summer monsoon responses to Asian aerosol forcing under different emission inventories,
660   *Advances in Climate Change Research*, https://doi.org/10.1016/j.accre.2022.02.008, 2022.
661   Wang Z., Lin L., Xu Y., Che H., Zhang X., Zhang H., Dong W., Wang C., Gui K. & Xie B.
662   Incorrect Asian aerosols affecting the attribution and projection of regional climate change in CMIP6
663   models, *npj Climate and Atmospheric Science.* 4(1), 2, 10.1038/s41612-020-00159-2, 2021.
664   Xia W., Wang Y., Chen S., Huang J., Wang B., Zhang G. J., Zhang Y., Liu X., Ma J., Gong
665   P., Jiang Y., Wu M., Xue J., Wei L. & Zhang T. Double Trouble of Air Pollution by Anthropogenic
666   Dust, *Environmental Science & Technology.* 56(2), 761-769, 10.1021/acs.est.1c04779, 2022.
667   Zheng B., Tong D., Li M., Liu F., Hong C., Geng G., Li H., Li X., Peng L., Qi J., Yan L.,
668   Zhang Y., Zhao H., Zheng Y., He K. & Zhang Q. Trends in China's anthropogenic emissions since
669   2010 as the consequence of clean air actions, *Atmos. Chem. Phys.* 18(19), 14095-14111, 10.5194/acp-
670   18-14095-2018, 2018.

671
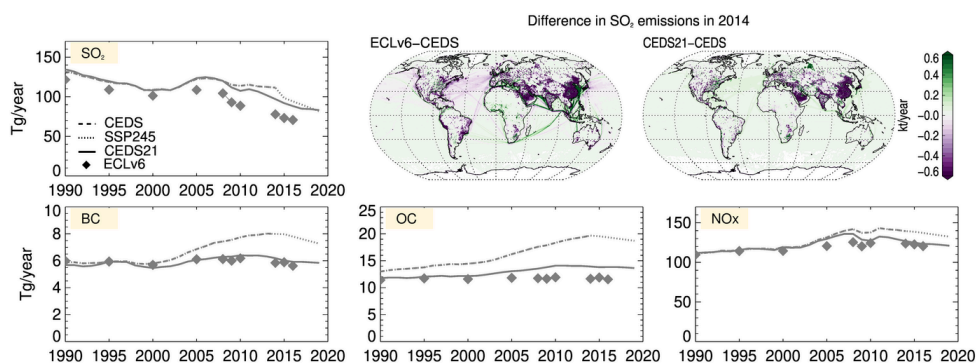
Figures:

Figure 1 *Global total anthropogenic emissions of SO₂, BC, OC, and NOx in the CEDS21, ECLv6, CEDS17 inventories, for the period 1990 to the most recent inventory year (2019, 2016 and 2014, respectively). Dotted lines show emissions from the SSP2-4.5 scenario, linearly interpolated from 2015 to 2019. The maps show the difference in SO2 emissions in 2014, the most recent common year*
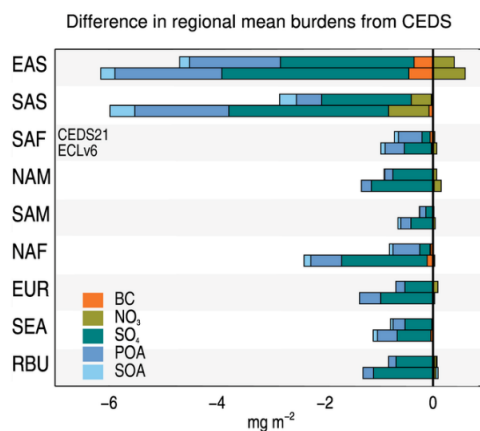
Figure 2 *Absolute difference in regional mean burden of the key anthropogenic aerosol species between simulations with CEDS21 and CEDS (upper bar) and ECLv6 and CEDS (lower bar). Regions are the same as in Lund et al. (2019): EAS = East Asia, SAS = South Asia, SAF = Sub-Saharan Africa, NAM = North America, SAM = South America, NAF = North Africa and the Middle East, EUR = Europe, SEA = South East Asia, RBU = Russia.*

691

692
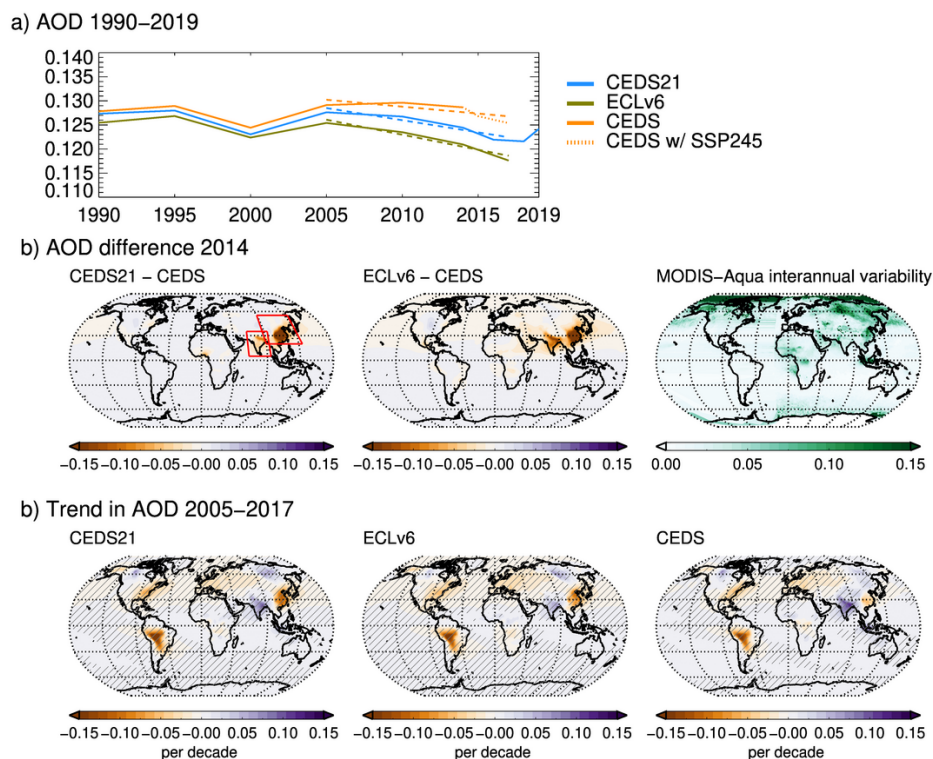
Figure 3: a) Global mean total AOD simulated with emissions from the CEDS21, ECLv6 and CEDS inventories. In the case of CEDS, the timeseries is extended from 2014 to 2017 using SSP2-4.5 emissions. Dashed lines show the linear 2005-2017 trend, defined as statistically significant from no trend when the linear Pearsons correlation coefficient is significant at the 0.05 level. b) Difference in AOD between the two inventories and CEDS in 2014, i.e. the last year of historical emissions in CEDS. Also shown is the interannual variability in MODIS AOD. c) Regional linear trends in AOD over 2005-2017 with the three different emission inventories.

700

701
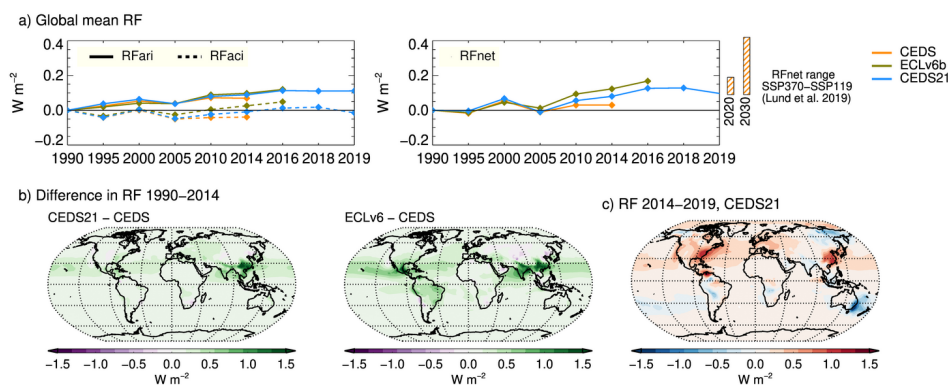
Figure 4: a) RFari and RFaci (left) and RFnet (RFari+RFaci) relative to 1990 under the CEDS21,
ECLv6, and CEDS emission inventories. The vertical bars to the right show the range in RFnet in 2020
and 2030 (relative to 1990) estimated with the SSP1-1.9 and SSP3-7.0 emissions (adapted from Lund et
al. (2019)). b) Difference in RFnet in 2014 relative to 1990 between simulations with ECLv6 and CEDS
emissions. c) The RFnet in 2019 relative to 2014 with CEDS21.
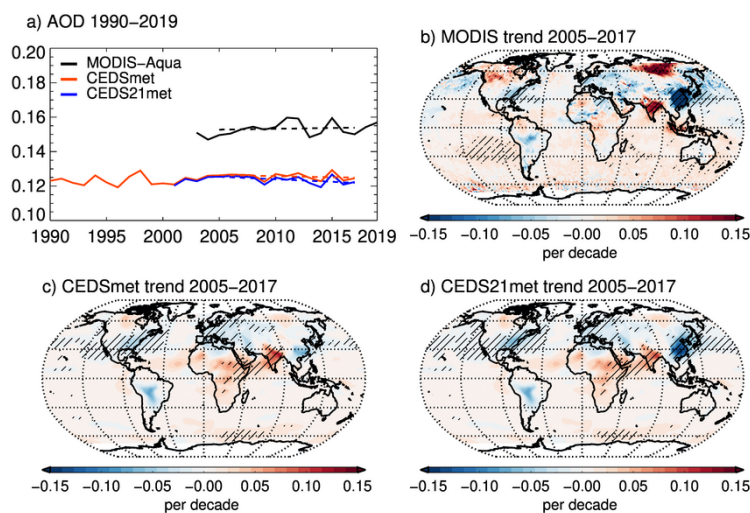
Figure 5: a) Global, annual mean AOD from MODIS-Aqua and the OsloCTM3 over the 1990-2019
period. Note that data north and south of 70° is excluded here due to the limited MODIS-Aqua coverage.
Dashed lines show linear trend from 2005 to 2017. b-d) Spatially resolved linear trends in observed and
simulated AOD. Hatching indicates where the linear trend is significantly different from zero at the 0.05
level.
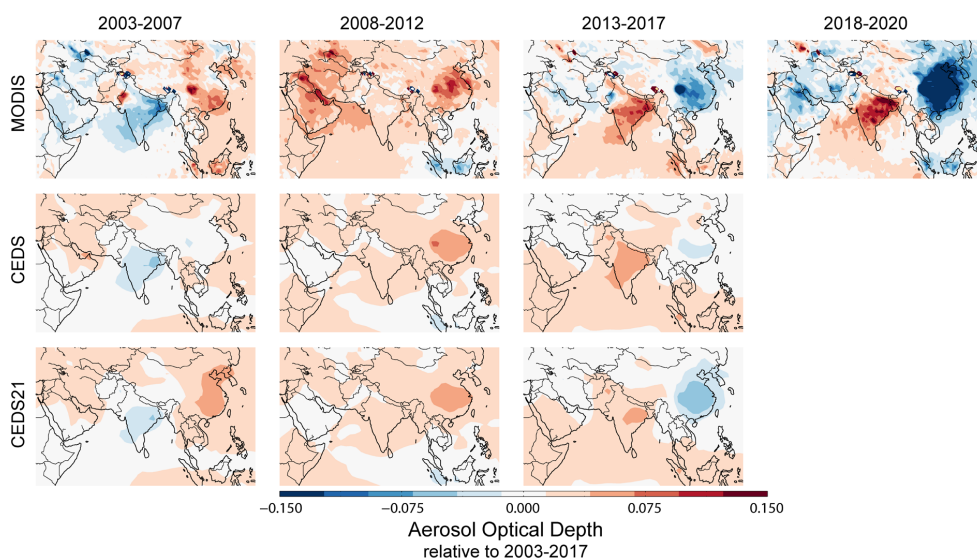
Figure 6: Evolution of AOD over South and East Asia, and the Middle East, over the period 2003-2020. All panels show five-year average deviations from the period 2003-2017, except the rightmost MODIS-Aqua panel which show the three-year average deviation (same baseline). The top row shows retrievals from MODIS Aqua; the two bottom rows show model calculations with OsloCTM3 based on the CEDS and CEDS21 emission inventories.